Available online at www.sciencedirect.com
ScienceDirect
Trans. Nonferrous Met. Soc. China 26(2016) 1163−1169
Transactions of Nonferrous Metals Society of China
www.tnmsc.cn

Oxidation behavior of RE-modified nickel-based superalloy between 950 °C and 1150 °C in air

Long-fei LIU, Shu-sen WU, Yang CHEN, Shu-lin LÜ

State Key Laboratory of Materials Processing and Die and Mould Technology, Huazhong University of Science and Technology, Wuhan 430074, China

Received 6 March 2015; accepted 31 August 2015

Abstract: A new Ni-based superalloy Ni48Cr28W5Co3Mn1Si1.6 was developed and the influence of a trace amount of rare earth (RE) metal addition on the oxidation resistance of this alloy was investigated. Isothermal oxidation behavior was investigated at 950−1150 °C in air, and then analyzed using scanning electronic microscopy and X-ray diffraction. The results showed that oxidation mass gain kinetics of the samples with and without RE elements follow the parabolic law. The effect of 0.20% RE on oxidation resistance is relatively small, and the oxidation rate constant of the alloy modified with 0.20% RE addition decreases by 5.9%−9.0%. Oxidation at 950−1150 °C for 100 h results in the formation of $MnCr_2O_4$, Cr_2O_3 and SiO_2. A continuous and protective $MnCr_2O_4$ spinel layer forms as outer layer. The continuous middle oxide layer is confirmed to be Cr_2O_3, and the innermost layer consists of discontinuous SiO_2.

Key words: Ni-based superalloy; rare earth element; high temperature oxidation; multi-layered oxides

1 Introduction

Owing to excellent high-temperature strength and oxidation resistance, Ni-based superalloys are commonly used for high temperature applications [1]. Especially in compact strip production of steel, the conveyor roller in the furnace for the hot-steel billet is normally made of Ni-based superalloy [2]. Therefore, improving the high-temperature oxidation resistance is an important direction of alloy development of Ni-based superalloys [3].

The Ni48Cr28W5 superalloy is a German standard Ni-based superalloy, the main components are Ni−Cr−Fe−W, and the Ni content is about 48%. In this study, a new Ni-based superalloy and its processing method are developed, which is modified from Ni48Cr28W5 by adding 3% Co, 1% Mn, 1% Si and a trace amount of rare-earth(RE) metals. This Ni48 alloy may be mainly used for the hearth roller in a soaking furnace in a short continuous-casting and rolling process of a steel product line in which the temperature reaches 1150 °C, thus a high temperature oxidation experiment is designed. To date, oxidation experiment has been rarely carried out at such high temperature for this kind of Ni-based alloy [4−6].

Generally, Ni-based superalloys exposed to high temperature and an oxygen-containing environment will produce oxides on the surface, such as Ta_2O_5, WO_3, TiO_2, Cr_2O_3 and Al_2O_3 [7−11]. However, Cr_2O_3 oxide can effectively obstruct the base material from further oxidation, reduce the rate of oxidation, and thus enhance the high temperature oxidation resistance [12]. Extensive studies of the oxidation behavior of Ni-based alloys have been published by a number of investigators. Alloys in this system with low Cr contents show internal oxidation of Cr forming Cr_2O_3 islands within a matrix of almost pure Ni [13]. An outer scale of NiO is formed with an inner layer, sometimes porous, of NiO containing $NiCr_2O_4$ islands. With Cr contents above the critical value, a protective Cr_2O_3 layer which covers the whole surface will be formed. The critical Cr content required to develop a chromia layer on Ni−Cr alloys is about 20% Cr [14]. HUSSAIN et al [15] investigated the oxidation behavior of a commercial Ni-based superalloy Hastelloy C−4 at 600 °C. They found that the oxidation kinetics obeyed the parabolic rate law, but were linear at the very beginning. LITZ et al [16] investigated the oxidation behavior of IN738 and IN939 alloys at 700, 900 and 1100 °C, and found that Cr_2O_3 formed when the Cr

Corresponding author: Shu-sen WU; Tel: +86-27-87556262; E-mail: ssw636@hust.edu.cn
DOI: 10.1016/S1003-6326(16)64215-2

content of the alloy was greater than 15% and Al content was less than 3%, the oxide film was nearly the same for two kinds of alloys.

It is now well established that small additions of reactive elements, such as Y, Hf, and Ce, substantially improve the adherence of chromia and alumina scales to alloy substrates. While the effects produced by the reactive elements are widely known, the mechanisms whereby they improve oxidation resistance are not completely understood. Over the last 50 years a number of mechanisms have been proposed: reactive elements acting as vacancy sinks to suppress void formation at the alloy−oxide interface, formation of oxide pegs at the alloy−oxide interface, alteration of the growth mechanism of the oxide resulting in reduced growth stresses.

Recent research on the oxidation of Ni-based superalloys focused on the role of microalloying in the oxidation kinetics and oxide layer formation. This work aims to investigate the effect of active elements (Mn, Si, RE) on oxidation reaction. The microstructure of oxide layers and the oxidation mechanism of 0.20% RE-added Ni48Cr28W5Co3Mn1Si1.6 (Ni48) alloy at 1150 °C has been aimed in the present study.

2 Experimental

The measured composition of the investigated Ni-based superalloy is shown in Table 1. The composition was measured by a PDA−7000 model optical emission spectrometer. The alloy to be used in this work was Ni48Cr28W5Co3Mn1Si1.6, which was prepared by using commercial pure Ni (99.95%), Cr (99.8%), Co (99.95%), and several master alloys: Fe−75%Si, rare-earth ferrosilicon and Fe−65%Mn. The rare-earth ferrosilicon used contains 35% RE. The RE was composed of 65% Ce and 35% La. The materials were melted in a 50 kW induction furnace at 1550 °C. Cylindrical rods of 25 mm in diameter were prepared by pouring alloy melt into ZrO_2 investment casting moulds. Specimens of 20 mm × 20 mm × 4 mm were sectioned from the rods by electro-discharge machining for oxidation experiments. Square samples were then ground with SiC papers from 150 to 1200 grit, followed by surface polishing with 3 μm diamond paste. Isothermal oxidation tests of the specimens were carried out for different time (2, 5, 10, 25, 50, 75 and 100 h) at 950, 1050 and 1150 °C. Each temperature corresponded to an independent sample, the accuracy of the balance was 0.1 mg, in order to determine the oxidation process with increasing oxidation time of Ni48 alloy.

Table 1 Composition of Ni-based superalloy (mass fraction, %)

Co	Fe	Cr	Si	W	Mn	C	Ni
3.14	13.78	28.15	1.63	4.86	0.99	0.14	Bal.

The morphology of the formed oxide layers of cross-section and surface was investigated using scanning electron microscopy (Quanta 200). In order to determine the chemical compositions across a given cross-section, energy dispersive X-ray spectroscopy (Oxford Instrument Inc.) measurements were carried out. The crystalline phases in the oxide layers were determined using X-ray diffraction (XRD, Philips X'pert).

3 Results and discussion

3.1 Morphology of matrix

The samples were made by an investment casting method in atmospheric environment. The moulds of casting rods were cooled in air, so the grain size was relatively large. Figure 1 shows the morphology of single-phase austenite Ni-based superalloy with some intermetallics along the grain boundaries.

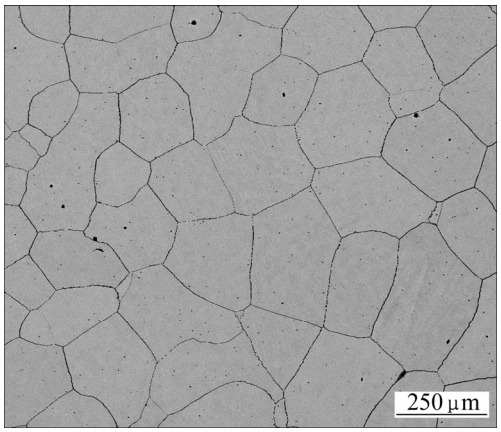

Fig. 1 SEM image of Ni48 alloy matrix

3.2 Oxidation kinetics

Figure 2 shows the isothermal oxidation kinetic curves of the Ni48 alloy with 0.20% RE or without RE at 950−1150 °C in air. Oxidation at higher temperatures leads to a higher mass gain per area ($\Delta m/A$). At the same temperature, mass gain of Ni48 alloy with 0.20% RE is smaller than that without RE addition. At lower temperatures, the effect of RE addition is not distinct, the scale is much thinner and the trend of spallation is not obvious. At higher temperatures (1050 °C and 1150 °C), the effect of RE is more obvious but still quite small. After 100 h oxidation, mass gain of Ni48 alloy with 0.20% RE addition is 3.6% lower compared with that of RE-free Ni48 alloy at 950 °C. This difference increases to 5.9% at 1050 °C, and at 1150 °C, this difference reaches 7.5%.

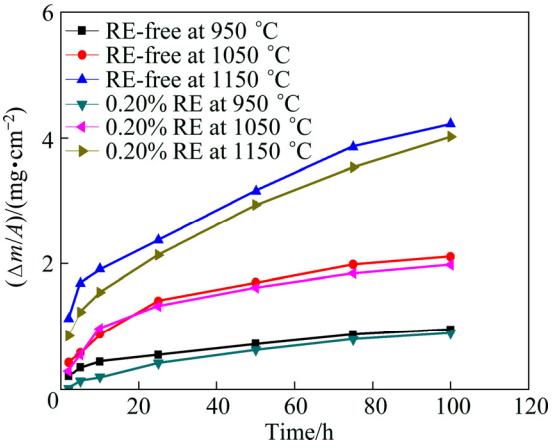

Fig. 2 Mass gain ($\Delta m/A$) of Ni48 alloy with 0.20% RE or without RE oxidized for 100 h at 1050−1250 °C

Isothermal oxidation kinetics of all specimens follows a parabolic law. The curves can be fitted by a straight line, which represents parabolic rate constant k. The rate constant, k, is described by the following equation:

$$\left(\frac{\Delta m}{A}\right)^2 = kt \tag{1}$$

where Δm is the mass change, A is the surface area of the specimen, k is the parabolic rate constant, and t is the oxidation time. The parabolic rate constants and the correlation coefficient are listed in Table 2. The parabolic rate constant can be described by the Arrhenius equation:

$$k = k_0 \exp\left(\frac{-Q}{RT}\right) \tag{2}$$

where k_0 is the pre-exponential factor, Q is the activation energy, R is the gas constant, and T is the temperature.

The slope of a linear regression-fitted line of $(\Delta m/A)^2$ versus t plot is shown in Fig. 3, which indicates the parabolic nature of oxidation kinetics.

Table 2 Oxidation rate constant (K_p) of Ni48 alloy with two different contents of rare earth

Specimen	Temperature/°C	K_p/(mg^2·cm^{-4}·h^{-1})	Q_p/(kJ·mol^{-1})
0.20% RE	950	7.99×10^{-3}	219.3
	1050	3.90×10^{-2}	
	1150	1.68×10^{-1}	
RE-free	950	9.47×10^{-3}	213.7
	1050	4.36×10^{-2}	
	1150	1.76×10^{-1}	

According to the data in Table 2, the oxidation rate constants of the 0.20% RE-added Ni48 alloy decreased by 15.6%, 10.6% and 4.6% at 950, 1050, 1150 °C, respectively, as compared with that of the Ni48 alloy without RE. The effect of 0.20% RE on oxidation resistance is small.

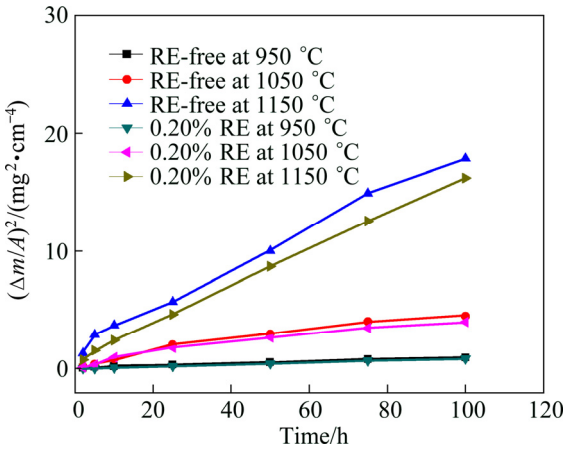

Fig. 3 Square of mass gain versus oxidation time showing parabolic nature of kinetic curve

The activation energies of RE-free specimens and 0.20% RE-added specimens are 213.7 and 219.3 kJ/mol, respectively. Both the activation energies of two kinds of specimens are extremely close to the diffusion activation of Cr^{3+} which is 259 kJ/mol. Based on this, we can predict that the oxidation process is Cr^{3+} ion-diffusion controlled.

3.3 Microstructure of oxide layers after 100 h isothermal oxidation

The macroscopic surface morphologies of the RE-free specimen and the 0.20% RE-added specimen after 100 h oxidation at 1150 °C are shown in Fig. 4. As can be seen in Fig. 4, the spallation ratio of the 0.20% RE-added specimen (Fig. 4(b)) is significantly smaller than that of the RE-free one (Fig. 4(a)). Figure 4 has been analyzed by the Zeiss micro-image analysis & process software, and the analysis shows that the spallation ratios of 0.20% RE-added specimens and RE-free specimens are 21% and 55%, respectively. The spallation ratio of the 0.20% RE-added specimen is significantly smaller than that of the RE-free sample. The addition of RE element to this chromia-forming alloy slows the diffusion of chromium through the scales. As a result, scale growth is mainly due to the inward diffusion of oxygen. To the extent that oxide scales are thinner, their susceptibility to spallation is lessened. RE also has a strong affinity for sulfur, which desulfurizes the alloy, forming sulphide particles, and preventing sulfur from contaminating the scale−alloy interface.

The microscopic surface morphologies of the RE-free specimen and the 0.20% RE-added specimen after 100 h oxidation at 1150 °C are shown in Fig. 5. As can be seen in Fig. 5, the surface morphologies of two kinds of specimens are nearly the same. In both images, the surfaces are divided into three layers (A, B,

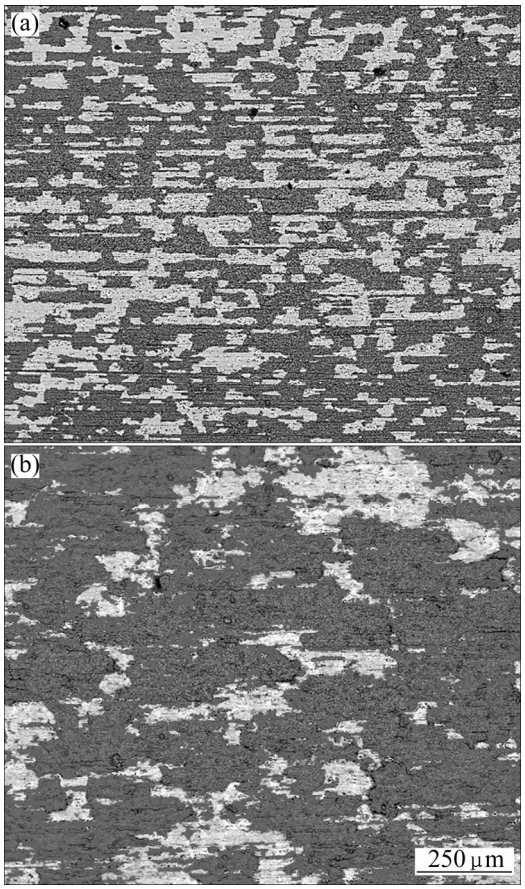

Fig. 4 SEM images of surfaces of Ni48 alloy specimens after 100 h oxidation at 1150 °C: (a) RE-free; (b) 0.20% RE

C). The parts *A* and *B* in Fig. 5 correspond to the darker part in Fig. 4, while part *C* in Fig. 5 corresponds to the lighter part in Fig. 4. The average crystal size of Fig. 5(c) is about 3.2 μm. The corresponding EDX spectra of parts *A*, *B* and *C* in Fig. 5 are shown in Table 3.

Combining SEM images in Fig. 5 and semi-quantitative EDS result in Table 3, the outmost layer of the oxide layer consists of Mn−Cr-containing oxides (part *A* in Fig. 5), and the underneath spinel structure is compact oxide layer of Cr-rich oxide (part *B* in Fig. 5), and the innermost layer is porous Si-rich oxide (part *C* in Fig. 5). At 1150 °C, the surface morphologies of RE-free Ni48 and 0.20% RE-added Ni48 are nearly the same. The trace amount and the high reactivity of the RE elements lead to poor detectability, thus it is failed to detect the existence of RE elements after the oxidation experiments.

After 100 h isothermal oxidation at 1150 °C in air, the SEM images of cross-sections are presented in Fig. 6. The cross-sectional image of RE-free specimen is shown in Fig. 6(a), and the cross-sectional image of 0.20% RE specimen is shown in Fig. 6(b). As can be seen from Fig. 6, mean oxide layer thickness of the RE-free Ni48 specimens is larger compared with that of 0.20% RE

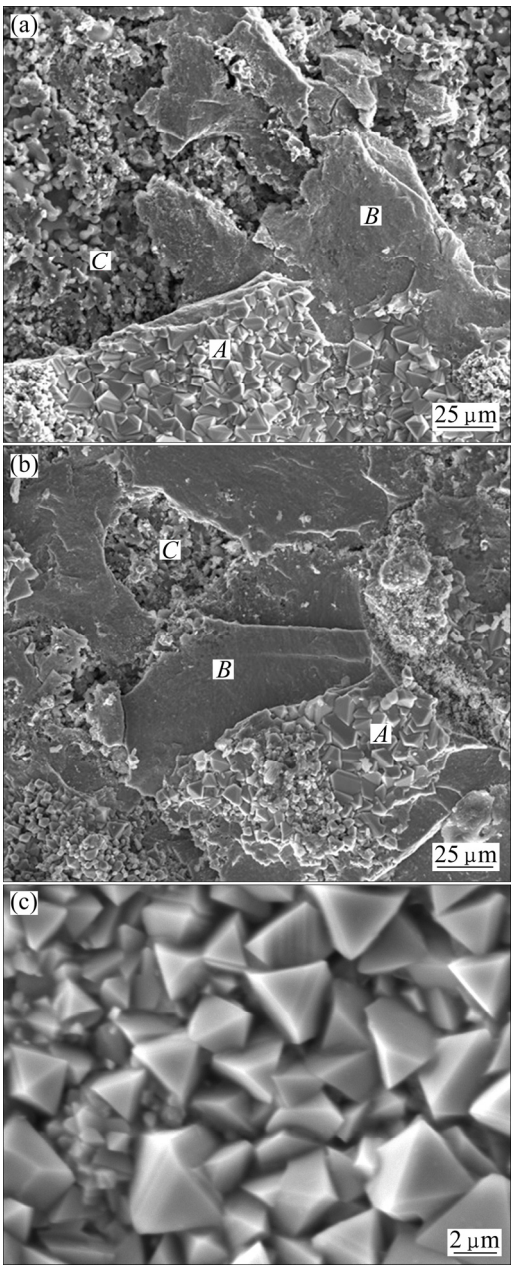

Fig. 5 SEM images of surfaces of Ni48 alloy specimens after 100 h oxidation at 1150 °C: (a) RE-free; (b) 0.20% RE; (c) Partial enlarged image of 0.20% RE

Table 3 EDX results of RE-free and added 0.20% RE Ni48 alloy at 1150 °C for 100 h (mole fraction, %)

Element	RE-free			0.20% RE		
	Part *A*	Part *B*	Part *C*	Part *A*	Part *B*	Part *C*
O	55.28	38.86	52.69	52.31	38.07	47.72
Cr	30.98	60.15	04.56	31.74	61.93	20.12
Mn	14.74			17.95		
Si		00.98	34.28			22.39
Ni			06.06			06.23
Fe			02.41			02.54

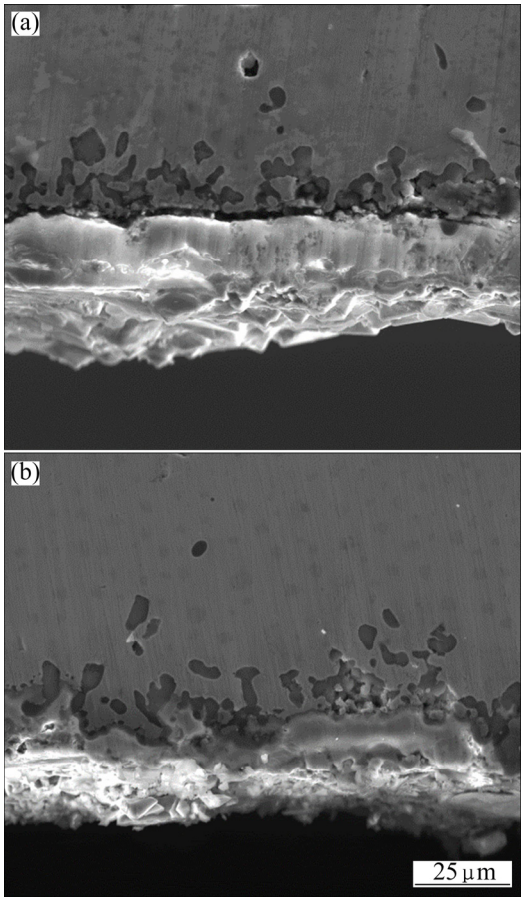

Fig. 6 Cross-sectional SEM images of Ni48 alloy specimens after 100 h oxidation at 1150 °C: (a) RE-free; (b) 0.20% RE

specimens after 100 h oxidation test at 1150 °C, and the rates of SiO_2 globular attack of the RE-free Ni48 alloy specimens are higher than those of the 0.20% RE specimens at the same temperature after 100 h oxidation.

Figures 7 and 8 are the map scanning images of the cross-sections in Figs. 6(a) and (b), respectively. It can be seen in Figs. 7 and 8 that the outermost oxide layers consist of oxides containing Cr and Mn, the middle oxide layers consist of Cr and O, and the inner oxide layers are confirmed to be mostly SiO_2. EDX maps of O, Si, Mn and Cr can be used to measure the average thickness of the oxide layer quantitatively, and the mean oxide layer thicknesses of the investigated alloys are shown in Table 4.

As shown in Table 4, each layer of RE-free specimen is little thicker than that in 0.20% RE specimen. The addition of RE element to this chromia-forming alloy slows the diffusion of chromium through the scales. As a result, scale growth is mainly due to the inward diffusion of oxygen. To the extent that oxide scales are thinner, their susceptibility to spallation is lessened.

The oxide layer was collected and analyzed by X-ray diffraction in order to identify the compounds, and the result is shown in Fig. 9. It can be judged from the Fig. 9 that the dominant constituent of the oxide layer is $MnCr_2O_4$ spinel and Cr_2O_3. The XRD patterns show a similar tendency that the intensity of $MnCr_2O_4$ spinel and Cr_2O_3 gradually increases with the increase of oxidation time. The peak of SiO_2 disappears due to the amorphous state.

3.4 Mechanism of multi-oxide layers formation

As mentioned above, the main reaction products in the oxide scale are SiO_2, Cr_2O_3 and spinel-type $MnCr_2O_4$ phases, which can be understood thermodynamically. The following reactions will occur according to the Ellingham−Richardson diagram [2]:

$$\frac{4}{3}Cr + O_2(g) = \frac{2}{3}Cr_2O_3(s),\ \Delta G_T^{\Theta} = -753.12 + 0.1826T \quad (3)$$

$$Si + O_2(g) = SiO_2(s),\ \Delta G_T^{\Theta} = -856.3 + 0.1825T \quad (4)$$

$$2Mn + O_2(g) = 2MnO(s),\ \Delta G_T^{\Theta} = -725.8 + 0.1498T \quad (5)$$

$MnCr_2O_4$ spinel is formed from MnO and Cr_2O_3 according to the following reaction:

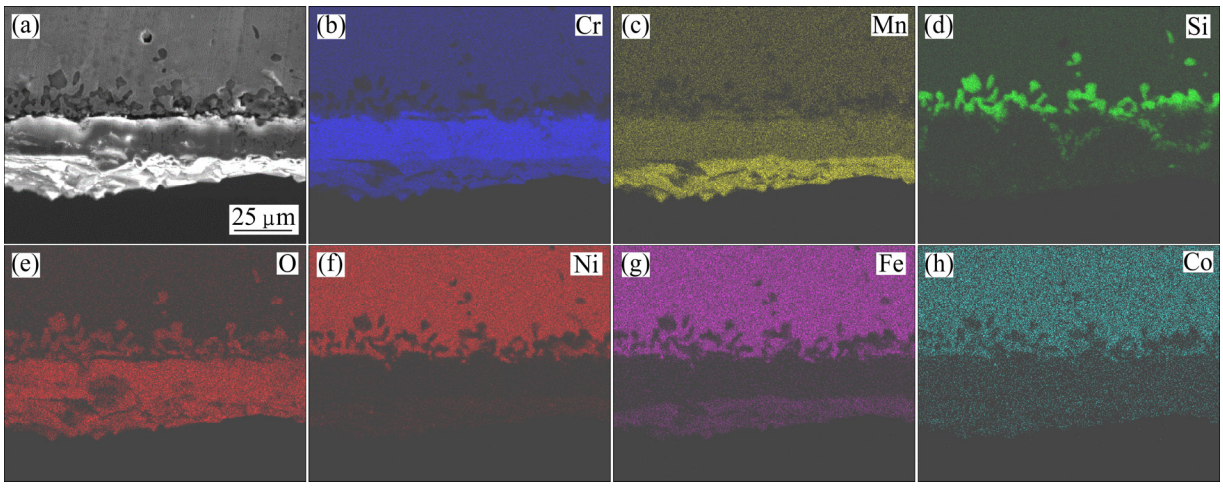

Fig. 7 EDX maps of RE-free Ni48 alloy oxidized at 1150 °C for 100 h

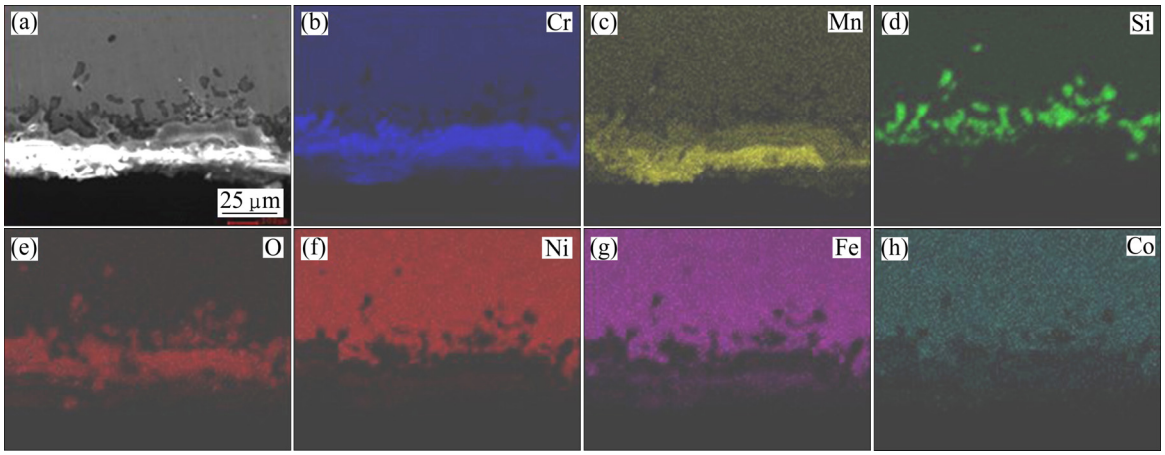

Fig. 8 EDX maps of 0.20% RE-added Ni48 alloy oxidized at 1150 °C for 100 h

Table 4 Mean oxide layer thickness of Ni48 alloys oxidized for 100 h

Alloy	Temperature/ °C	Mean outermost oxide layer thickness/μm	Mean middle oxide layer thickness/μm	Mean inner oxide layer thickness/μm
RE-free	1150	15.9	14.9	20.1
0.20% RE	1150	13.8	11.8	17.9

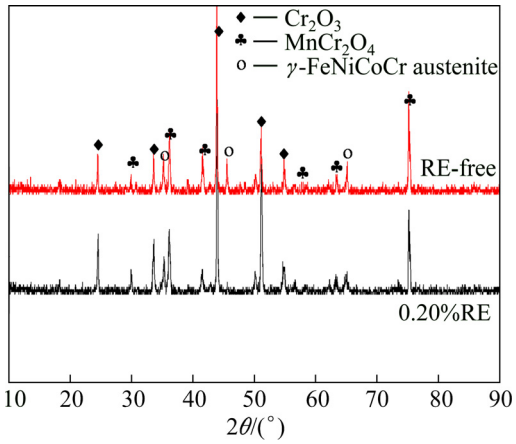

Fig. 9 XRD patterns of surface products of RE-free and 0.20% RE-added Ni48 alloys oxidized at 1150 °C in air for 100 h

$$MnO + Cr_2O_3 = MnCr_2O_4(s),$$
$$\Delta G_T^{\Theta} = -1469.2 + 0.2798T \quad (6)$$

These equations suggest that the free energies, ΔG_T^{Θ}, of Cr_2O_3, SiO_2 and $MnCr_2O_4$ are negative, thus providing theoretical base to understand the appearance of Cr_2O_3, SiO_2 and $MnCr_2O_4$. Moreover, the ΔG_T^{Θ} value in Eq. (4) proves that $MnCr_2O_4$ spinel is formed from MnO and Cr_2O_3 spontaneously. While exposed to air in the experimental temperature range, both Cr and Mn in the Ni48 alloy are simultaneously oxidized to form Cr_2O_3 and MnO initially, and then Cr_2O_3 and MnO react with each other to form $MnCr_2O_4$, as $\Delta G_{MnCr_2O_4}^{\Theta}$ is more negative than either ΔG_{MnO}^{Θ} or $\Delta G_{Cr_2O_3}^{\Theta}$. $MnCr_2O_4$ is thermodynamically more stable than both Cr_2O_3 and MnO.

The oxidation process consists of multiple parts. At the very beginning, the O_2 molecules are adsorbed onto the surface of the specimen and decompose into O atoms. These O atoms diffuse into the substrate, and choose the element which has the highest reactive activity to form the oxides. The contents of Mn and Si are much lower than that of Cr in this alloy, so the Cr element has the highest reactive activity. In this stage, a dense Cr_2O_3 layer is formed at scale−substrate interface, and the oxidation kinetics is controlled by the chemical reaction of Cr atoms and O atoms at the gas−alloy interface, and the oxidation rate of this stage is rapid. The crystal nuclei of Cr_2O_3 grow into a thin compact oxidation layer as the reaction progresses. This compact oxidation layer cuts off the adsorption process of O atoms and the oxidation rate decreases obviously. Then, the oxidation goes to the next stage, and the oxidation starts to be controlled by the inward diffusion of O atoms and outward diffusion of Cr and Mn atoms. Mn ions diffusion is orders of magnitude faster than that of Cr ions in Cr_2O_3. $MnCr_2O_4$ forms at the gas−scale interface, and thickens as a result of Mn ions diffusion through Cr_2O_3 layer. As this stage goes on, the content of Cr and Mn at substrate−scale decreases to a very low level, and there is a depletion zone of Cr and Mn, which can be seen in Figs. 7 and 8. There is a dark band between Cr_2O_3 layer and SiO_2 globular attack in Cr and Mn EDX map scan images of Figs. 7 and 8. Owing to the depletion zone of Cr and Mn, the oxidation rate is relatively slow. At the meantime, the O atoms enter into the alloy matrix,

and then Si and RE elements are oxidized simultaneously. RE elements are more reactive than Si, and they will be oxidized first. Then, SiO_2 grows on the heterogeneity nucleus of REOs, and the REOs enhance the adhesion between substrate and SiO_2 layer. As the multi-oxide layers become thicker, the diffusion-controlled reaction becomes slow, causing decrease in oxidation rate.

4 Conclusions

1) After 100 h oxidation experiments at the temperatures of 950, 1050, 1150 °C, oxidation mass gain of the samples with 0.20% RE or RE-free obeys the secondary parabolic law. The oxidation rate constants of the alloy with RE decrease by 15.6%, 10.6% and 4.6% at 950, 1050, 1150 °C, respectively, as compared with that of the alloy without RE. The spallation ratio of the 0.20% RE-added specimen is significantly smaller than that of the RE-free sample.

2) After 100 h oxidation, a continuous and protective $MnCr_2O_4$ spinel layer forms as outer layer, the continuous middle oxide layer is confirmed to be Cr_2O_3, and the innermost layer consists of discontinuous SiO_2. The diameter of $MnCr_2O_4$ spinel crystal is around 3.2 μm and it can strongly improve the oxidation resistance.

Acknowledgments

This work was funded by the foundation of HUST−WISCO Joint Laboratory. The authors would also like to express their appreciation to the Analytical and Testing Centre, Huazhong University of Science and Technology, China.

References

[1] SIMS C T, HAGEL W C. The superalloys [M]. New York: John Wiley & Sons, 1972.

[2] SIMS C T, STOLOFF N S, HAGEL W C. The superalloys [M]. New York: John Wiley & Sons, 1987.

[3] BELTRAN A M. Superalloys II [M]. New York: John Wiley & Sons, 1987.

[4] LAWLESS K R. The oxidation of metals [J]. Reports on Progress in Physics, 1974, 37: 231−316.

[5] CABRERA N, MOTT N F. Theory of the oxidation of metals [J]. Reports on Progress in Physics, 1949, 12: 163−184.

[6] YUAN Liang, HU Rui, ZHANG Tie-bang, LI Jin-shan, ZHANG Xiao-qing. Oxidation behavior of Hastelloy C-2000 superalloy at 800 °C and 1000 °C [J]. Transactions of Nonferrous Metals Society of China, 2015, 25(1): 354−362.

[7] SHI Zhen-xue, LI Jia-rong, LIU Shi-zhong. Isothermal oxidation behavior of single crystal superalloy DD6 [J]. Transactions of Nonferrous Metals Society of China, 2012, 22(3): 534−538.

[8] JIANG S M, LI H Q, MA J, XU C Z, GONG J, SUN C. High temperature corrosion behaviour of a gradient NiCoCrAlYSi coating II: Oxidation and hot corrosion [J]. Corrosion Science, 2010, 52: 2316−2322.

[9] ZHANG X R, DMITRIJ Z, DAVID W S. Characterization of film properties on the Ni−Cr−Mo alloy C-2000 [J]. Electrochimica Acta, 2013, 89: 814−822.

[10] LI Bao-zeng, WANG Qing, WANG Ying-min, QIANG Jian-bing, LI Xiao-na, JI Chun-jun. A ferrite stainless steel Cr27Mo6Al3Cu with oxidation resistance [J]. Materials & Design, 2012, 40: 171−175.

[11] MCDANIELS R L, CHEN L, STEWARD R, LIAW P K, BUCHANAN R A, WHITE S, LIAW K, KLARSTROM D L. The strain-controlled fatigue behavior and modeling of Hastelloy C-2000 superalloy [J]. Materials Science and Engineering A, 2011, 528: 3952−3960.

[12] CHEN G F, LOU H Y. Effect of nanocrystallization on the oxidation behavior of a Ni−8Cr−3.5Al alloy [J]. Oxidation of Metals, 2000, 54: 155−162.

[13] CHEN J H, ROGERS P M, LITTLE J A. Oxidation behavior of several chromia-forming commercial nickel-base superalloys [J]. Oxidation of Metals, 1997, 47: 381−410.

[14] LEDJEFF K, RAHMEL A, SCHORR M, WEISS J. Influence of metal grain growth on the oxidation behavior of a 25Cr−20Ni steel [J]. Oxidation of Metals, 1981, 15: 485−493.

[15] HUSSAIN N, SHAHID K A, KHAN I H. Oxidation of high-temperature alloys (superalloys) at elevated temperatures in air [J]. Oxidation of Metals, 1994, 41: 251−269.

[16] LITZ J, RAHMEL A, SCHORR M. Scale formation on the Ni-base superalloys IN 939 and IN 738 LC [J]. Oxidation of Metals, 1989, 32: 167−184.

一种添加微量混合稀土镍基高温合金在 950~1150 °C 下的氧化行为

刘龙飞，吴树森，陈 阳，吕书林

华中科技大学 材料成形与模具技术国家重点实验室，武汉 430074

摘 要：开发了一种新型镍基高温合金(Ni48Cr28W5Co3Mn1Si1.6)并研究微量混合稀土对其氧化性能的影响。在950~1150 °C下进行100 h的等温氧化试验，并对试样进行SEM和XRD分析。结果表明，添加和不添加混合稀土的试样，其氧化增重均满足抛物线规律。加入少量混合稀土对氧化增重影响很小，加入0.20% 稀土的试样，其氧化速率常数降低5.9%~9.0%。常温氧化100 h后，氧化产物为$MnCr_2O_4$、Cr_2O_3和SiO_2。氧化层共3层，最外层为连续有保护性的$MnCr_2O_4$尖晶石层，中间层是致密的Cr_2O_3，最内层为不连续的SiO_2层。

关键词：镍基高温合金；稀土元素；高温氧化；多层氧化膜

(Edited by Xiang-qun LI)